DOI: 10.13009/EUCASS2023-218
Aerospace Europe Conference 2023 – 10TH EUCASS – 9TH CEAS

Modeling of the cathode air supply for a pressurized hydrogen fuel cell system in airborne applications

Daniel Frank†, Christiane Bauer* and Caroline Willich**
** Institute for Energy Conversion and Storage, Universität Ulm*
Albert-Einstein-Allee 47, 89081 Ulm, Germany
daniel.frank@uni-ulm.de – christiane.bauer@uni-ulm.de – caroline.willich@uni-ulm.de
† Corresponding Author

Abstract

The cathode air supply of a fuel cell system is modelled as a compressor-volume-throttle system with individual plena and spool dynamics. For both the throttle valve and the compressor, transfer functions describing their transient behavior have been established. The parameters of the model have been identified. The model was implemented and validated against measurement data. The results show concurrence of the compressor speed, valve opening angle, pressure rise, and mass flow in simulation and measurement. The model can be used in the development of an automatic control system, and is low in computational effort.

1 Introduction

The use of hydrogen for propulsion in aircraft promises to reduce the climate impact of aviation by up to 90% [1] and is seen as a suitable aviation fuel for short and intermediate distances [2]. Using PEM fuel cells in hybrid-electric planes has attracted much attention in the last years [3,4], however, in order to obtain high power and efficiency while operating PEM fuel cells at high altitudes, pressurizing the cathode inlet air is necessary.

In previously presented work, a cathode air supply system was designed and tested [5]. It consists of an electrically driven centrifugal compressor, a temperature management unit, a humidification unit and a throttle valve at the outlet. Figure 1 shows an updated design of this earlier presented air supply system.

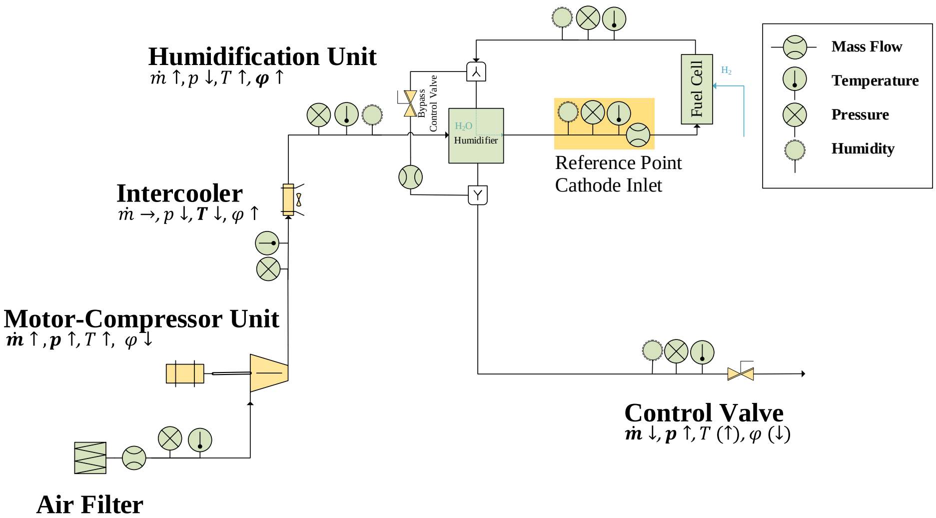

Figure 1: Design of the cathode air supply system.

The automatic control utilizes a decentralized control strategy with pilot control for cathode pressure and mass flow regulation, manipulating compressor speed and control valve opening. The functionality of the system was demonstrated, stable and unstable modes of operation in steady state and transient operation were identified, but the transient behavior could not be predicted in this previous work. Consequently, a transient model of the cathode air supply system was developed, in order to obtain a better understanding of the dynamic system behavior and to facilitate the development of more sophisticated control strategies.

DOI: 10.13009/EUCASS2023-218

2 Compression system model

The transient characteristics of the air supply system are mainly defined by the characteristics of the key components, compressor and throttle valve, as well as the by the internal volume of the compression system. Hence, a model of a compressor-volume-throttle system with spool dynamics, presented by Gravdahl & Egeland [6], is utilized as a basis for the work presented here.

The compression system model of Gravdahl & Egeland [6], being an extension of the model presented by Greitzer [7,8], consists of three differential equations, which describe the change in plenum pressure p_p, compressor mass flow m_c and rotational impeller velocity ω, see Equations (1) – (3):

$$\frac{dp_p}{dt} = \frac{a_{01}^2}{V_p}(m_c - m_t) \tag{1}$$

$$\frac{dm_c}{dt} = \frac{A_1}{L_c}(p_2 - p_p) \tag{2}$$

$$\frac{d\omega}{dt} = \frac{1}{I}(\tau_t - \tau_c) \tag{3}$$

Here, a_{01} designates the inlet stagnation sonic velocity, V_p the plenum volume, m_t the throttle mass flow, A_1 the area of the impeller eye, L_c the length of the compressor and ducts, p_2 the pressure downstream of the compressor, I the spool moment of inertia, τ_t the drive torque, and τ_c the compressor torque.

In the original model [6], the fuel cell cathode inlet pressure is considered to be the evenly distributed internal pressure p_p of the overall plenum volume V_p. For the analysis presented here, the plenum volume is separated into the individual plena, as shown in Figure 2. This enables the model to predict pressures and mass flow rates of the individual components.

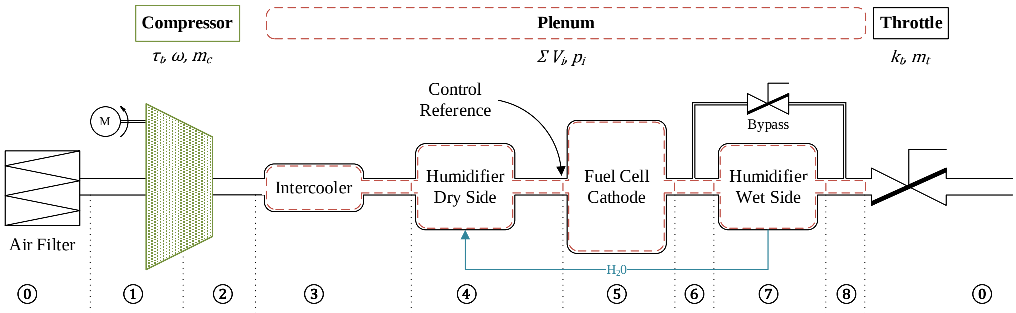

Figure 2: Cathode air supply system, modelled as compressor-volume-throttle system with multiple plena.

The introduction of separated plena changes the original model to Equations (4) – (6):

$$\frac{dp_3}{dt} = \frac{a_2^2}{V_3}(m_c - m_3) \tag{4}$$

$$\frac{dm_c}{dt} = \frac{A_1}{L_c}(p_2 - p_3) \tag{5}$$

$$\frac{d\omega}{dt} = \frac{1}{I}(\tau_t - \tau_c) \tag{6}$$

The change in mass flow rate and pressure within the plena are modelled with Equations (7) and (8). Similar approaches have been described by Barchewitz [9] and Smolarik *et al.* [10].

$$\frac{dm_i}{dt} = \frac{A_i}{L_i}\left(p_{i-1} - p_i - \mathrm{sign}(m_i)\,\Delta p_i(m_i)\right) \tag{7}$$

$$\frac{dp_i}{dt} = \frac{a_i^2}{V_i}\left(\sum m_{i,in} - \sum m_{i,out} + \sum m_{i,source}\right) \tag{8}$$

In the presented work, additional terms for the pressure loss Δp_i within each control volume V_i and mass sources or sinks $m_{i,source}$, such as the mass of the consumed hydrogen in the fuel cell, the addition or reduction of water in the humidifier or internal air leakage in the humidifier, have been introduced to the model.

DOI: 10.13009/EUCASS2023-218

3 Component models & parameter identification

The mass flow m_i and pressure p_i distribution in the compression system, as well as the compressor rotational speed ω can be calculated by solving the model Equations (4) – (8), if the properties and parameters of the individual components, mainly compressor and throttle valve, are known.

Identifying the appropriate set of parameter values in the model is necessary to quantitatively predict the transient behavior of the real system. The parameter set is specific for the chosen hardware. The presented parameter identification process was applied to an experimental setup using an EK10AA (Rotrex, DK) as motor-compressor-unit and APCs (Hyundai Kefico, KOR) as valves. Most of the parameters of the model were identified from hardware measurements, some were extracted from manufacturer datasheets.

The manipulated parameters in the compression system model (Equations (4) – (6)) are the drive torque τ_t and throttle gain k_t. In the real system these parameters cannot be controlled directly. τ_t is subject to the motor-inverter-unit of the compression system and its internal control law with the requested compressor speed ω_{req} as input parameter. k_t is a function of the valve opening angle ν and the differential pressure over the valve Δp. The valve movement follows an internal control law, that sets ν according to the requested valve opening angle ν_{req}. For both motor-inverter-unit and throttle valve, transfer functions need to be identified and implemented into the model.

3.1 Throttle valves model

The mass flow through the throttle valve and the bypass valve are modelled using Equations (9) and (10) [6,10], respectively, where p_0 is the ambient pressure, p_6 the pressure at the inlet of both the wet side of the humidifier and the bypass, p_8 the pressure upstream of the throttle valve and downstream of both the wet side of the humidifier and the bypass, k_t the throttle gain, and $k_{t,B}$ the gain of the bypass valve. During a flight mission, the ambient pressure p_0 will vary with the flight altitude.

$$m_t = k_t \operatorname{sign}(p_8 - p_0)\sqrt{|p_8 - p_0|} \tag{9}$$

$$m_{6,B} = k_{t,B} \operatorname{sign}(p_6 - p_8)\sqrt{|p_6 - p_8|} \tag{10}$$

As the same hardware is used for the throttle valve and the bypass valve, the same function is used for k_t and $k_{t,B}$. k_t depends on the valve opening angle ν and the pressure difference $\Delta p = p_8 - p_0$.

$$k_t(\nu, \Delta p) = k_{t,B}(\nu, \Delta p) \tag{11}$$

For the identification of k_t as a function ν and Δp, the mass flow m_t was measured, varying the valve opening angle ν and the pressure difference Δp. From the definition in Equation (9), k_t is calculated as given in Equation (12).

$$k_t(\nu, \Delta p) = \frac{m_t}{\operatorname{sign}(p_8 - p_0)\sqrt{|p_8 - p_0|}} \tag{12}$$

k_t is then modelled as a polynomial function as given in Equation (13).

$$k_t(\nu, \Delta p) = p_{00} + p_{10} * \nu + p_{01} * \Delta p + p_{20} * \nu^2 + p_{11} * \nu * \Delta p \tag{13}$$

A graphical representation of the result is shown in Figure 3, where the measured base points are marked with asterisks ($*$) and the fitted polynomial is plotted as the surface.

DOI: 10.13009/EUCASS2023-218

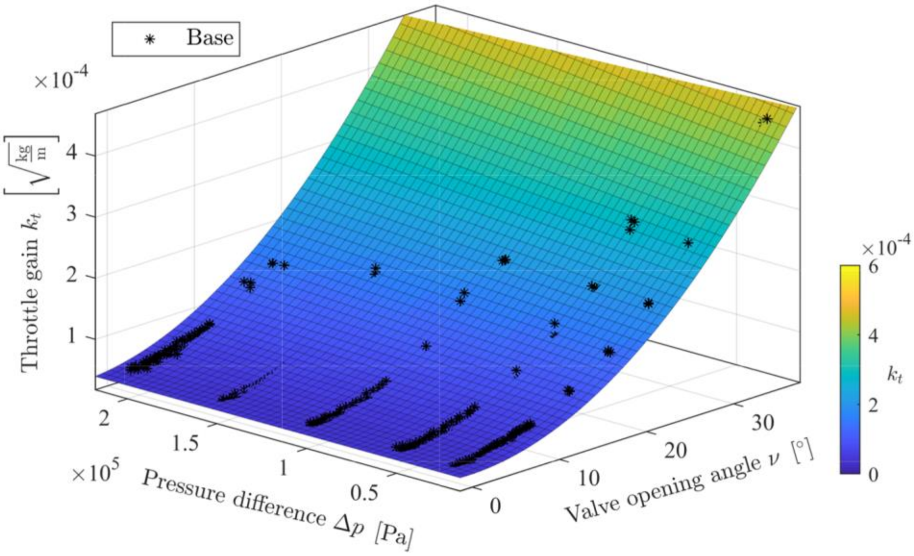

Figure 3: The throttle gain is a function of the pressure difference over the valve and the valve opening angle.

The movement of the valve as the response to a change in the requested valve opening angle ν_{req} is modelled as a first-order lag with time delay (see Figure 4). The parameters of the transfer function in the frequency domain are identified from measurement data utilizing the MATLAB® System Identification Toolbox [11]. It is assumed, that during the change of the valve opening angle ν, k_t is only depending on ν and Δp.

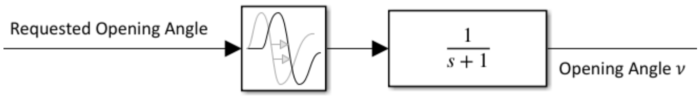

Figure 4: The valve movement is modelled as a first-order lag with time delay in the frequency domain.

Figure 5 shows a comparison of measured data and simulated data with the previously identified parameter set for an exemplary opening movement of the valve and an exemplary closing movement.

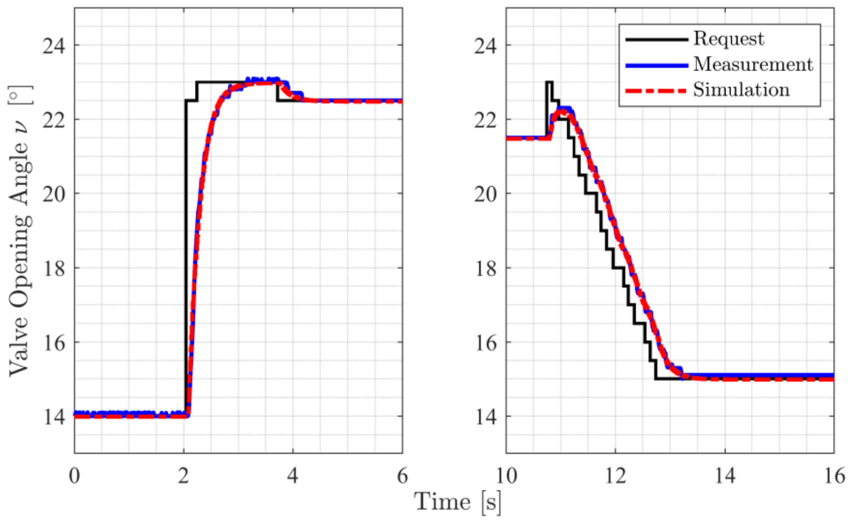

Figure 5: Comparison of the requested, simulated and measured valve opening angle during an opening (left) and a closing movement (right).

For both modes of operation, opening and closing equally, a very good representation of the valve's actual movement is achieved. The simulated data produces a slightly smoother signal than the measured data. The comparison of the requested, simulated and measured signal in Figure 5 from $t = 14$ s exhibits a dead-band behavior of the measured signal with a bandwidth of $0.2°$. This is considered neglectable for the presented work.

DOI: 10.13009/EUCASS2023-218

3.2 Compressor pressure rise model

The pressure downstream of the compressor p_2 is calculated according to Equation (14) [6].

$$p_2 = p_1 \cdot \left(1 + \frac{\eta_i \, \Delta h_{0c,ideal}}{T_1 c_p}\right)^{\frac{\kappa}{\kappa - 1}} \tag{14}$$

The product $T_1 c_p$ is the specific enthalpy of the compressor intake air, with the fluid temperature at the compressor inlet T_1 and the specific heat capacity of the fluid c_p. The ideal specific enthalpy transferred to the fluid $\Delta h_{0c,ideal}$ is calculated as given in Equation (15) [6]. The isentropic efficiency η_i accounts for the non-ideal enthalpy transfer.

$$\Delta h_{0c,ideal} = \sigma U_2^2 \tag{15}$$

The tangential speed of the impeller tips U_2 is calculated from compressor speed ω and the diameter of the impeller at the tip D_2, see Equation (16).

$$U_2 = \frac{1}{2} D_2 \omega \tag{16}$$

The slip factor σ is defined as in Equation (17) [6],

$$\sigma = \frac{C_{\theta 2}}{U_2} \tag{17}$$

where $C_{\theta 2}$ is the tangential fluid velocity at the rotor exit. The slip factor σ accounts for the tangential gas velocity at the impeller exit not being equal to U_2. Therefore, less enthalpy can be transferred to the fluid.

In order to calculate the pressure rise in the simulation, the distribution of η_i and σ over the operational map of the compressor need to be extracted from manufacturer datasheets or from measurement data by measuring compressor mass flow m_c, inlet and outlet pressures p_1 and p_2, and temperatures T_1 and T_2 at varying compressor speeds and throttling.

If the measured compressor inlet pressures p_1 and temperatures T_1 deviate from the respective reference values p_{ref} and T_{ref}, both m_c and ω must be corrected to m_{corr} and ω_{corr} with Equations (18) and (19) [12], in order to obtain the appropriate values for η_i and σ.

$$m_{corr} = \frac{m_c \sqrt{T_1 / T_{ref}}}{p_1 / p_{ref}} \tag{18}$$

$$\omega_{corr} = \frac{\omega}{\sqrt{T_1 / T_{ref}}} \tag{19}$$

The determination of the efficiency map and the slip factor map as functions of corrected mass flow and corrected compressor speed, $\eta_i(m_{corr}, \omega_{corr})$ and $\sigma(m_{corr}, \omega_{corr})$, is described is the following sections.

3.2.1 Determination of the efficiency map

The non-ideal enthalpy transfer to the fluid is characterized by the isentropic efficiency η_i, which is defined in Equation (20), assuming constant fluid properties during the compression. T_2 is the measured fluid temperature after the compression in the real system, $T_{2,s}$ the theoretical fluid temperature for an isentropic compression, as given in Equation (21).

$$\eta_i = \frac{\Delta h_{0c,ideal}}{\Delta h_{0c,real}} = \frac{T_{2,s} - T_1}{T_2 - T_1} \tag{20}$$

$$T_{2,s} = T_1 \left(\frac{p_2}{p_1}\right)^{\frac{\kappa - 1}{\kappa}} \tag{21}$$

Figure 6 shows the compressor efficiency map of the used compressor [13], as a function of the corrected mass flow m_{corr} and the corrected compressor speed ω_{corr}. Between the base points, that were extracted from the datasheet [13], linear interpolation is applied.

DOI: 10.13009/EUCASS2023-218

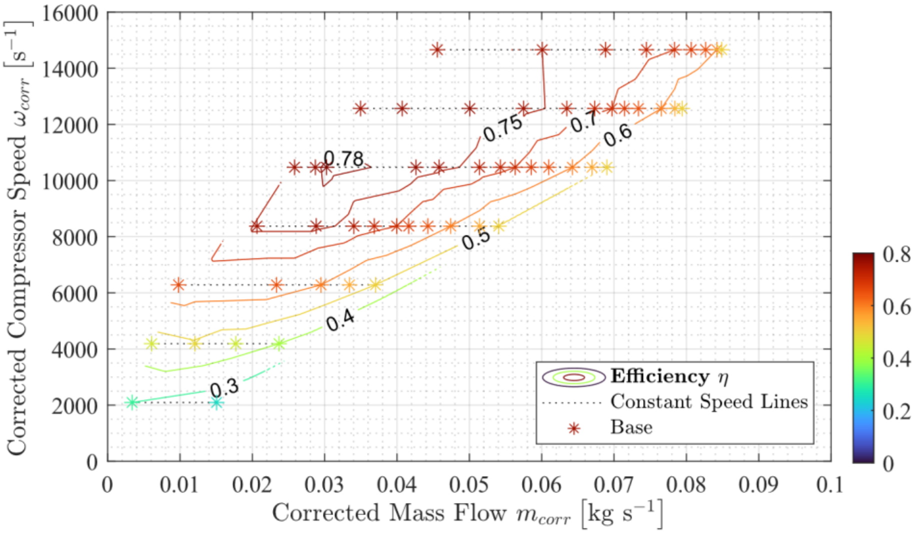

Figure 6: Compressor efficiency distribution extracted from manufacturer data [13] in the range of $\eta_i = 0.25 \,..\, 0.79$.

If necessary, the quality of the efficiency map, and therefore of the simulation results, can be improved by narrowing the grid of base points, or by applying an interpolation method that better represents the efficiency distribution.

3.2.2 Determination of the slip factor

The enthalpy transfer to the fluid is in general less than its theoretical maximum, which is defined by the compressor speed (see Equations (15) - (17)). The slip factor is used to quantify the actual enthalpy transfer. After solving Equations (14) and (15) for σ, the slip factor can be calculated with Equation (22), if the efficiency distribution is known.

$$\sigma = \left(\left(\frac{p_2}{p_1}\right)^{\frac{\kappa-1}{\kappa}} - 1\right)\frac{T_1 c_p}{\eta_i\, U_2^2} \tag{22}$$

Applying Equation (22) to the data shown in Figure 6 generates a compressor slip factor map as shown in Figure 7. The pressure ratio $\frac{p_2}{p_1}$ and the compressor inlet temperature T_1 are given in the data provided by the manufacturer [13]. Between the base points, linear interpolation is used.

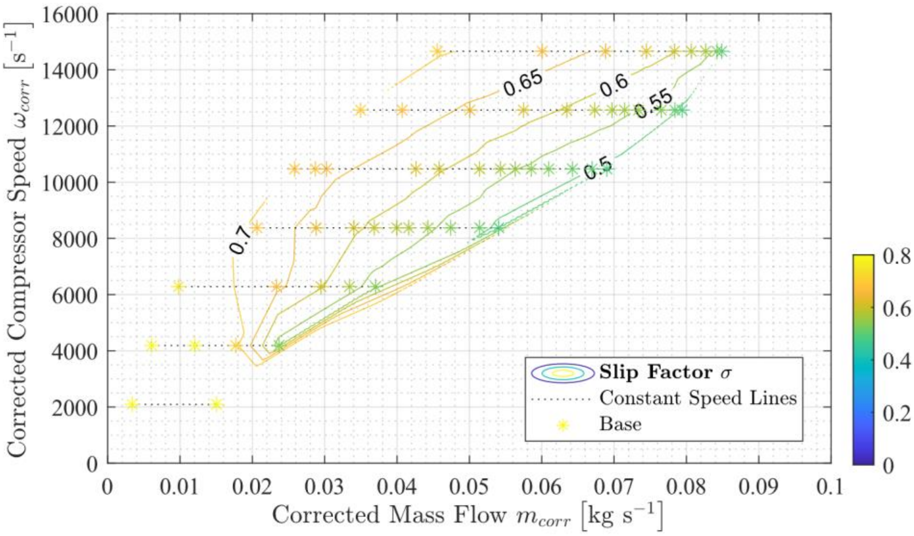

Figure 7: Compressor slip factor distribution calculated from manufacturer data [13] in the range of $\sigma = 0.49 \,..\, 0.82$.

It is to be noted, that the slip factor is not a constant, but a function $\sigma(m_{corr}, \omega_{corr})$, which ranges from $\sigma = 0.49$ at higher mass flows to $\sigma = 0.82$ at lower mass flows for the used compressor.

DOI: 10.13009/EUCASS2023-218

3.3 Compressor spool dynamics

In the model, Equation (6) describes the change in rotational velocity depending on the balance of the driving torque of the spool τ_t and the aerodynamic breaking torque τ_c, as well as the spool moment of inertia I.

From Euler's turbine equation, the compressor torque τ_c is derived as in Equation (23) [6].

$$\tau_c = \frac{1}{2}|m_c|D_2\sigma U_2, \tag{23}$$

The drive torque τ_t is the difference of the torque provided by the motor-inverter-unit τ_m and the mechanical loss torque τ_f, see Equation (24).

$$\tau_t = \tau_m - \tau_f \tag{24}$$

With the introduction of the mechanical loss coefficient μ_f, τ_f is calculated as is given in Equation (25).

$$\tau_f = \mu_f \omega \tag{25}$$

Equation (6) then becomes Equation (26).

$$\frac{d\omega}{dt} = \frac{1}{I}\left(\tau_m - \mu_f\omega - \frac{1}{4}|m_c|D_2^2\sigma\omega\right) \tag{26}$$

In order to simulate the spool dynamics, the mechanical loss coefficient μ_f, the moment of inertia I and a transfer function for τ_m need to be identified.

3.3.1 Mechanical loss coefficient

The mechanical loss coefficient accounts for loss mechanisms which are depending on the compressor speed, including friction, and is calculated with Equation (27) after solving Equation (26) for μ_f.

$$\mu_f = \frac{1}{\omega}\left(\tau_m - \frac{d\omega}{dt}I - \frac{1}{4}|m_c|D_2^2\sigma\omega\right) \tag{27}$$

The value of μ_f was determined from measurement data. Choosing measurement data with constant compressor speed, and therefore $\frac{d\omega}{dt} = 0$, as is shown the shaded area in Figure 8, allows for the direct calculation of μ_f, using the measured values of the motor torque τ_m and the rotational velocity ω of the compressor.

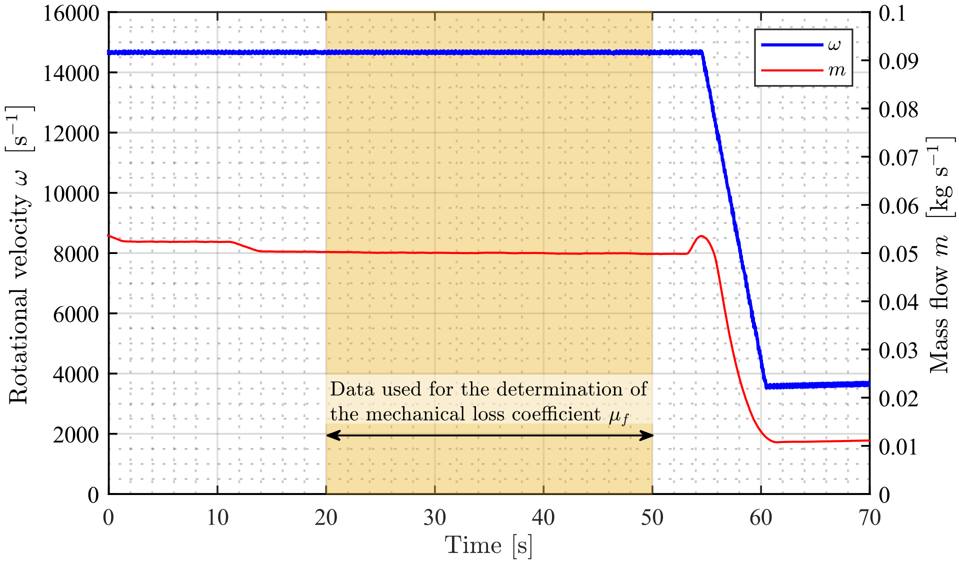

Figure 8: Measurement data at constant compressor speed used for the calculation of the mechanical loss coefficient μ_f.

As the measured rotational velocity ω and mass flow m_c are fluctuating, a low pass filter has been applied to the data before calculating the mechanical loss coefficient μ_f.

3.3.2 Moment of inertia

The moment of inertia I of the compressor spool is calculated from Equation (26) as is given in Equation (28).

$$I = \frac{1}{\frac{d\omega}{dt}}\left(\tau_m - \mu_f\omega - \tfrac{1}{4}|m_c|D_2^2\sigma\omega\right) \tag{28}$$

In order to identify I, the deceleration of the compressor is measured, where $\tau_m = 0$, and a section of the curve is chosen where $\omega \gg 0$ and $\omega(t)$ can be approximated as linear ($\frac{d\omega}{dt} = \text{const.}$), as is shown by the shaded area in Figure 9.

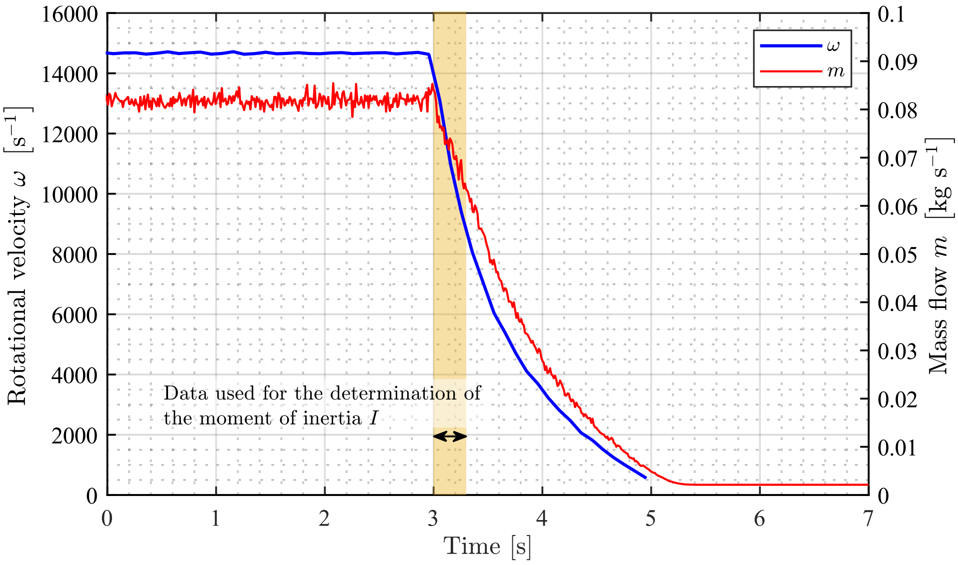

Figure 9: Measurement data at $\frac{d\omega}{dt} = const.$ used for the calculation of the moment of inertia I.

Since ω and m_c by default vary during the measurement and exhibit fluctuating signals, I was calculated for every sample of the measurement data and afterwards averaged.

3.3.3 Motor torque

The motor torque τ_m is mainly determined by the inverter's internal control law and limited by the hardware's torque limits and scaled by the inverse of the gear ratio. Extracting the control law from the inverter and introducing a time delay T_t results in a to some extent idealized transfer function for the motor torque τ_m output of the motor-inverter-combination. The implementation in the model is shown in Figure 10.

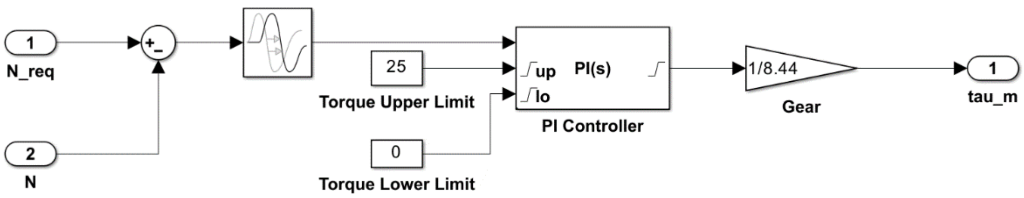

Figure 10: Idealized representation of the motor torque τ_m output of the motor-inverter-unit as a response to the requested compressor speed $N_{req} = {}^{\omega_{req}}/_{2\pi} * 60\frac{s}{min}$.

The control difference $N_{req} - N$ is applied to the PI-controller with a time delay T_t. From the control law, the resulting torque is calculated within the set limits, and scaled by the inverse of the gear ratio, resulting in the motor torque τ_m. While solving Equation (6), the speed limits of the compressor are applied.

DOI: 10.13009/EUCASS2023-218

3.4 Identified parameters

In the previous sections the component models and the procedure of identifying the essential parameters was outlined. The described identification method has been applied to the chosen hardware for the setup. The resulting parameters are summarized in Table 1.

COMPONENT	PARAMETER	SYMBOL	VALUE
COMPRESSOR	Efficiency	η_i	0.25 .. 0.79, see Figure 6
	Slip factor	σ	0.49 .. 0.82, see Figure 7
	Moment of inertia	I	3.9218×10^{-4} kg m^2
	Mechanical loss coefficient	μ_f	8.1889×10^{-5} Nm s
	Diameter at impeller tip	D_2	0.054 m
	PI controller	P	0.03125
		$I * Ts$	0.25
		T_t	0.02 s
		Lower Limit	0 Nm
		Upper Limit	25 Nm
	Gear ratio		8.44
	Speed limit	Lower	0 rpm
		Upper	140 krpm
VALVE	Coefficients of $k_t(\nu, \Delta p)$	p_{00}	3.862×10^{-5}
		p_{10}	1.461×10^{-7}
		p_{01}	1.434×10^{-11}
		p_{20}	3.03×10^{-7}
		p_{11}	9.443×10^{-12}
	Transfer function	Numerator	5.1234
		Denominator	$s + 5.1295$
		Time Delay	0.035 s
AIR PROPERTIES	Specific heat coefficient	c_p	$1010 \frac{\mathrm{J}}{\mathrm{kg\,K}}$
	Isentropic exponent	κ	1.4

Table 1: Summary of parameters used in the simulation.

The identified parameter set was validated against measurement data from the hardware setup. The validation process and results are described in the following chapter.

4 Validation

The overall goal of the presented work was to be able to predict the transient behavior of a cathode air supply system. The system model, including the component models and the identified parameters, has been implemented in SIMULINK® (R2022b) [14]. The hardware, for which the parameters where identified, was set up and tested in a test rig [5]. For both model and hardware setup, the input parameters to the compression system are the requested rotational speed of the compressor ω_{req} and the requested valve opening angle ν_{req}.With the hardware setup, first measurement data has been produced, where an automatic controller calculated time-varying compressor speed and valve opening angle requests. These logged requests, as well as the compressor inlet pressures p_1 and temperatures T_1, were used as inputs to the model, and the simulation results were compared to the measured values from the test rig. Figure 11 shows a comparison of requested, simulated and measured time-varying rotational velocity, valve opening angle, compressor outlet pressure and compressor mass flow.

The first and second graph of Figure 11 show a very good agreement between the compressor speed and valve opening angle in simulation and measurement, indicating that the identified I, μ_f and σ, and the transfer function of the motor-inverter-unit are consistent and suitable to simulate the spool movement, as well as a suitable identification of the valve transfer function.

The third graph of Figure 11 shows agreement of the simulated and measured compressor outlet pressure p_2. A deviation between the measurements and the simulation of approximately ± 0.1 bar at lower compressor outlet pressures can be seen. For higher outlet pressures the agreement is better, at approximately ± 0.04 bar. The fourth

DOI: 10.13009/EUCASS2023-218

graph shows the corresponding measured and simulated mass flow rate. Here, an offset of the simulation result towards lower mass flows can be seen. The observed discrepancies likely have two reasons.
First, the efficiency assumed in the simulation is too low for lower pressure ratios and compressor speeds, resulting in both lower mass flows and lower outlet pressures in the simulation, as can be seen in Figure 11 at times $t < 28$ s. To mitigate this, the efficiency distribution needs to be determined from measurement data.
Second, for higher pressure ratios and mass flows the throttle gain function of the valve needs refinement, as the simulated pressure is higher than the measured pressure, while the simulated mass flow is lower than the measured mass flow, as can be seen in Figure 11 at times $t = 30\,..\,66$ s.

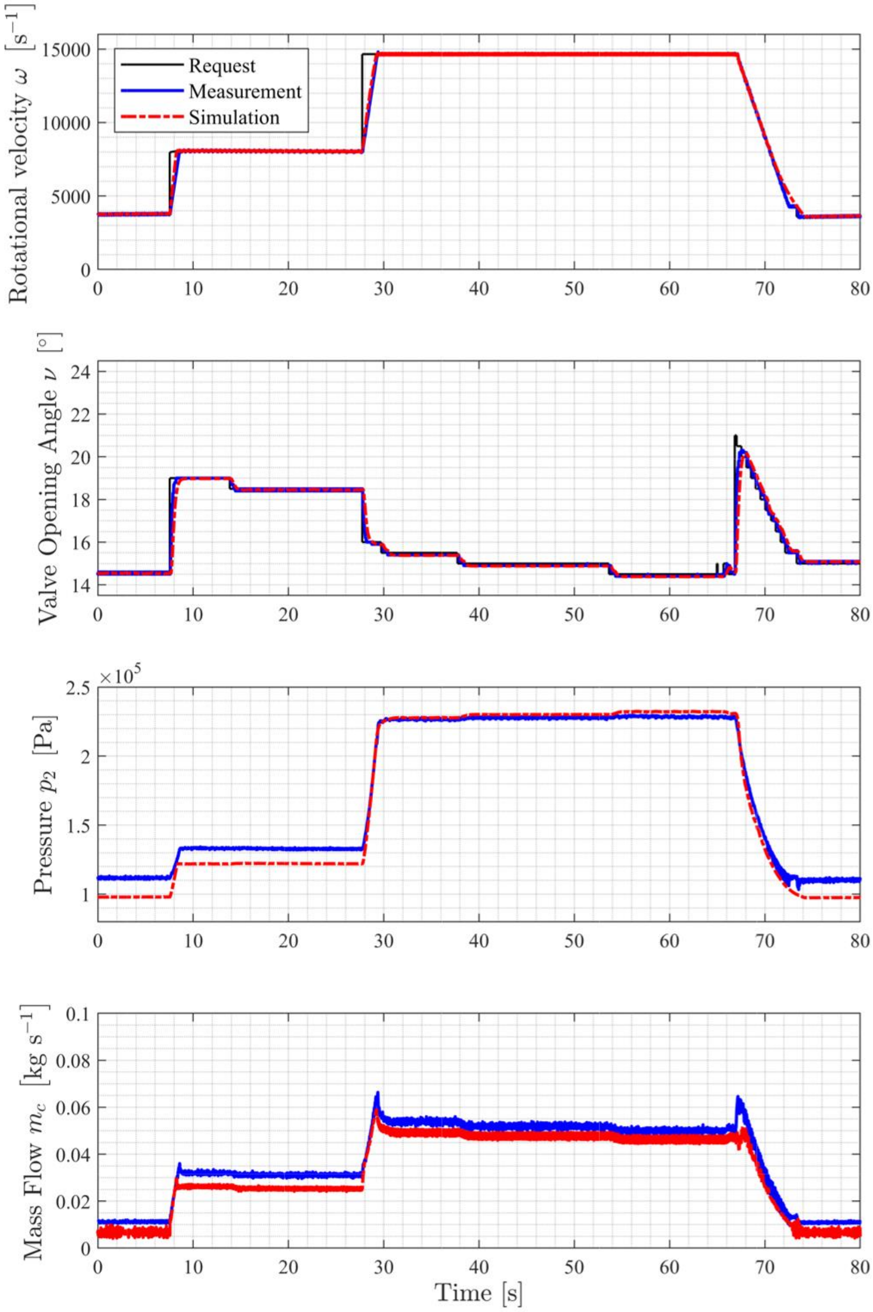

Figure 11: Comparison of simulated and measured time-varying rotational velocity, valve opening angle, compressor outlet pressure and compressor mass flow.

The presented model is able to predict the transient behavior of the cathode air supply system with the identified parameter set. The model can be used for the development of an automatic control system. It is low in computational effort with an achieved simulation pace of 11.86 on the used processing hardware [15].

DOI: 10.13009/EUCASS2023-218

5 Conclusion

A transient model of the cathode air supply of a PEM fuel cell system was developed. As basis, a model of a compressor-volume-throttle system with spool dynamics is utilized. For the analysis presented here, the plenum volume is separated into the individual plena. This enables the model to predict pressures and mass flow rates of the individual components. Additionally, terms for the pressure loss within each control volume and mass sources or sinks, such as the mass of the consumed hydrogen in the fuel cell, the addition or reduction of water or internal air leakage in the humidifier, have been introduced to the model.

For the throttle valve, a relation between differential pressure, valve opening angle and mass flow rate, as well as a transfer function describing the valve movement have been established.

For the compressor, the pressure rise is calculated from the efficiency and slip factor distribution, and the compressor speed. The compressor spool dynamics are described with the spool moment of inertia, a mechanical loss coefficient and a transfer function for the torque output of the motor-inverter-unit.

The parameters of the model have been identified from measurements and datasheets. The model was implemented and validated against measurement data, using the identified parameter set. The results show a very good agreement of the compressor speed and valve opening angle between simulation and measurement. The calculated pressure rises and mass flows also are in concurrence with the validation data. They show however some discrepancies, which point to the efficiency distribution of the compressor and the throttle valve gain function needing refinement for more accuracy in the simulated results.

The model describes the transient behavior of the air supply system well. It can be used further in the development of an automatic control system, and is low in computational effort.

References

[1] McKinsey & Company, Clean Sky 2 Joint Undertaking, Fuel Cells and Hydrogen 2 Joint Undertaking. Hydrogen-powered aviation: A fact-based study of hydrogen technology, economics, and climate impact by 2050. [November 29, 2022]; Available from: https://op.europa.eu/s/xfZc.

[2] Thomson R, Weichenhain U, Sachdeva N, Kaufmann M. Hydrogen: A future fuel for aviation? 2020.

[3] H2FLY GmbH. H2FLY realizes hydrogen-powered zero-emission aviation. Made in Stuttgart, GER; Available from: https://www.h2fly.de/.

[4] MTU Aero Engines AG. Flying fuel cell; Available from: https://www.mtu.de/technologies/clean-air-engine/flying-fuel-cell/.

[5] Frank D, Schröter J, Bauer C, Willich C. Development of a control strategy for an air supply module for pressurizing fuel cells in airborne applications. International Journal of Hydrogen Energy 2023. https://doi.org/10.1016/j.ijhydene.2023.05.204.

[6] Gravdahl JT, Egeland O. Centrifugal compressor surge and speed control. IEEE Transactions on Control Systems Technology 1999;7(5):567–79. https://doi.org/10.1109/87.784420.

[7] Greitzer EM. Surge and Rotating Stall in Axial Flow Compressors—Part I: Theoretical Compression System Model. Journal of Engineering for Power 1976;98(2):190–8. https://doi.org/10.1115/1.3446138.

[8] Greitzer EM. Surge and Rotating Stall in Axial Flow Compressors—Part II: Experimental Results and Comparison With Theory. Journal of Engineering for Power 1976;98(2):199–211. https://doi.org/10.1115/1.3446139.

[9] Barchewitz L. In-flight air supply system for PEM fuel cells; 2008.

[10] Smolarik L, Mudrončík D, Strbo M. Modeling and Control of Compression System. AMM 2014;693:110–6. https://doi.org/10.4028/www.scientific.net/AMM.693.110.

[11] The MathWorks Inc. MATLAB® System Identification Toolbox version: 10.0 (R2022b). Natick, Massachusetts, United States: The MathWorks Inc; 2022.

[12] Gravdahl JT, Egeland O. Compressor Surge and Rotating Stall. London: Springer London; 1999.

[13] Rotrex A/S. Technical Data Sheet EK10AA Range V1.40; Available from: https://rotrex-fuel-cell-compressor.com/fuel-cell-compressors/.

[14] The MathWorks Inc. SIMULINK® version: 10.6 (R2022b). Natick, Massachusetts, United States: The MathWorks Inc; 2022.

[15] Intel Corporation. Intel® Core™ i7-1185G7 Processor. [June 25, 2023]; Available from: https://ark.intel.com/content/www/us/en/ark/products/208664/intel-core-i71185g7-processor-12m-cache-up-to-4-80-ghz-with-ipu.html.